Physica Scripta

RECEIVED
26 April 2025

REVISED
25 June 2025

ACCEPTED FOR PUBLICATION
30 June 2025

PUBLISHED
10 July 2025

PAPER

Low-energy electron scattering on CN radical over a range of internuclear separations

He Su[1,*], **Jonathan Tennyson**[2,*], **Hong Zhang**[3], **Xinlu Cheng**[4], **Qunchao Fan**[1] **and Yangjun Yan**[1]

[1] School of Science, Key Laboratory of High Performance Scientific Computation, Xihua University, Chengdu, 610039, People's Republic of China
[2] Department of Physics and Astronomy, University College London, London, WC1E 6BT, United Kingdom
[3] College of Physics, Sichuan University, Chengdu, 610065, People's Republic of China
[4] Institute of Atomic and Molecular Physics, Sichuan University, Chengdu, 610065, People's Republic of China
[*] Authors to whom any correspondence should be addressed.

E-mail: suhe378@hotmail.com **and** j.tennyson@ucl.ac.uk

Keywords: electron scattering, electronic excitation, cyano radical, CN− resonance, R-matrix method

Supplementary material for this article is available online

Abstract

Low-energy electron scattering calculations on the open-shell CN radical are performed using the fixed-nucleus R-matrix method for several internuclear separations (R). The elastic, momentum transfer, differential and electronic excitation cross section are presented at various target and scattering models. We report five CN^- core-excited shape resonances lying above the first electronic excitation threshold, namely $^3\Sigma^+$, $1\,^3\Pi$, $2\,^3\Pi$, $^3\Sigma^-$ and $^1\Sigma^-$. The CN^- resonance curves are analyzed as a function of R, confirming that the resonances become narrower with increasing R and in general their energies drop; the $^3\Sigma^+$ resonance becomes bound for $R > 1.3918$ Å. The designation of these resonances are discussed. By the analysis of changing R, the difference on the magnitude of cross sections is prominent happening at the peak positions. The results obtained here provide a starting point for studies of electron-impact resonant vibration excitation and other CN^- resonance-driven phenomena in plasma.

1. Introduction

The cyano (CN) radical and its counterpart anion CN^- are fundamental molecules found in numerous environments, ranging from the sun's atmosphere to terrestrial plasmas. The CN rotational spectrum has been used to measure the temperature of the cosmic microwave background along different lines of sight [1, 2]. Information on low-energy electron scattering with molecule is important as such collisions can cause electronic excitation leading to observable emissions in plasma and astronomical environment. Notably the $A\,^2\Pi$ and $B\,^2\Sigma^+$ electronic excited state undergoes transition to the $X\,^2\Sigma^+$ ground state resulting in source of the 'CN red' [3] and 'CN violet' [4] electronic bands respectively, which are widely used to monitor CN, see [5] and references there in.

CN^- is one of a small number of anions observed in the interstellar medium (ISM) [6], while its origin and abundance are still disputed. The existence of negative ions in ISM was historically associated with radiative electron attachment. Recently Douguet *et al* [7] and Khamesian *et al* [8] investigated the formation of the CN^- ion by radiative electron attachment, who suggest that CN^- ions are unlikely to be formed by radiative electron attachment in the ISM. Harrison and Tennyson [9] suggested that the majority interstellar CN^- is likely formed by dissociative attachment to a CN containing species. The various possible paths to formation of C_nN^- species in the ISM were also proposed by Carelli *et al* [10]. More recently, Gao *el al* [11] provided experimental evidence that CN^- species are produced by dissociative electron attachment to BrCN; they assumed that the superexcited-state CN^{-**} are possibly produced by the electron attachment to CN radical, because of many low-energy electrons and free CN radicals in the interstellar space. In a study of the CN^- anion, Skomorowski *et al* [12] predict seven low-lying singlet and triplet resonances by employing the equation-of-motion coupled-

cluster method, and they classified these metastable states as shape resonances which correspond to valence $\pi \rightarrow \pi^*$ or $\sigma \rightarrow \pi^*$ excitation from the (bound) ground state of the anion.

A literature survey reveals only a few studies of electron impact on the open-shell CN molecule, especially ones that consider different geometry structures. Rotational excitation cross sections of CN by electron impact were calculated some time ago by Crawford *et al* [13] and Allison and Dalgarno [14]. Total ionization cross sections of the electron-impact on target CN was performed by Pandya *et al* [15] employing the Complex potential ionization contribution (CSP-ic) method, at incident energies from ionization threshold to 2 keV. Harrison and Tennyson [9] employed the R-matrix method [16, 17] to calculate bound and resonance states of CN^- at several internuclear separations, as well as elastic cross sections and electronic excitation cross sections in the equilibrium structure for electron scattering with CN in the ground $X\,^2\Sigma^+$ state. Subsequently, Harrison *et al* [2, 18] extended their work to treat explicitly spin-coupled rotational excitation cross sections and rate coefficients. Derouich *et al* [19] provided polarization transfer rates associated with the $A\,^2\Pi$ and $B\,^2\Sigma^+$ excited states. CN radicals are highly reactive and therefore difficult species to work with in the laboratory. Several groups measured the absolute cross sections for electron-impact detachment, ionization and dissociation of CN^- and CN^+ ions respectively [20–22]. The absolute photodetachment cross sections of CN^- were measured at an energy near the photodetachment threshold by Kumar *et al* [23]. To our knowledge, there are no available measurements of CN^- resonances and cross section for low-energy electron collision with the open-shell CN radical.

The fixed-nucleus R-matrix method [16, 17] can give accurate descriptions of elastic and inelastic processes in the low-energy scattering on *N*-containing molecules according to our previous studies [24–26]. The aim of this paper is to investigate electron collisions with CN radical for a range of internuclear distances by employing the R-matrix method for incident energy up to 10 eV. The formation of CN^- resonance along with elastic and electronic excitation cross sections were discussed as a function of C−N internuclear separation. The paper is organized as follows, section 2 introduces the R-matrix methodology, section 3 presents the target and scattering calculation details, then section 4 discusses the results for the studied collision processes. and finally, we present our concluding remarks and perspectives.

2. R-matrix methodology

The calculations reported in this work are performed using the fixed-nucleus R-matrix method the details of which can be found in the reviews [16, 17]. The electron-molecule scattering calculations were performed using the Quantemol Electron Collision (QEC) code [27], which runs both Molpro [28] for target models and the UK molecular R-matrix (UKRmol+) [29] code for scattering processes.

The fundamental idea underlying the R-matrix method is the division of configuration space into an inner and outer region which are separated by a sphere of radius $r = a$. The inner region is assumed to be sufficiently large contain to the electronic charge density of target *N*-electron target molecule; hence in this region there are $N+1$ indistinguishable electrons, where the $+1$ accounts for the scattering electron. In the inner region, short-range interactions such as exchange and electron–electron correlation must be explicitly treated. The results obtained in the inner region are fed to the outer region via the R-matrix which is constructed on the boundary. In outer region only the long-range mulitipole potentials are considered. Within the R-matrix sphere, the calculations start by considering the *N*-electron target problem. Then the *N*-electron target plus scattering electron calculation gives a full description of the target interacting with the scattering electron. The wave function of $N+1$ electron system in a fixed-nuclei approximation is expressed in the inner region as [16]:

$$\Psi_k^{N+1}(x_1, \ldots, x_{N+1}) = A\sum_{ij} a_{ijk}\varphi_i^N(x_1, \ldots, x_N)u_{ij}(x_{N+1}) + \sum_i b_{ik}\chi_i^{N+1}(x_1, \ldots, x_{N+1}) \quad (1)$$

Where *A* accounts for the anti-symmetrization operator which ensures that the Pauli principle is obeyed by the electrons. Coefficients a_{ijk} and b_{ik} are variational parameters which are determined as a result of the matrix diagonalization. φ_i^N is the wavefunction of the *i*th target state, and x_N is the spatial and spin coordinate of the *N*th target electron. u_{ij} are the continuum orbitals used to represent scattering electron. In equation (1), the first term defines the target plus continuum states. The second term provides short-range correlation effects in the form of the χ_i^{N+1} configurations which are L^2 multi-centered, square-integrable correlation configuration functions given by placing all electrons in target molecular orbitals. In our calculations, both target and continuum molecular orbitals were represented by linear combinations of Gaussian type orbital (GTOs).

In the outer region, solves energy-dependent scattering problem is by propagating the R-matrix which is built at the boundary of the R-matrix sphere using the inner region solution. This R-matrix is then matched to asymptotic solutions of Gailitis expansion [30] giving the *K*-matrix. The outer region calculations are rapid and can be repeated for many scattering energies. From *K*-matrices, one can obtain *T*-matrices, which are further

Table 1. CN ground $X\,^2\Sigma^+$ and $A\,^2\Pi$ target energies (in Hartree for the lowest state), excitation energies (in eV), dipole moments (μ in Debye) and electron affinities (in eV) for a range of internuclear separations (R, Å).

R	Method	$X\,^2\Sigma^+$	$A\,^2\Pi$	$B\,^2\Sigma^+$	μ	Electron affinity
0.9718	CAS(5,7)	−92.1840	2.639		1.962	3.477
	CAS(9,9)	−92.2404	3.120	3.321	1.750	3.412
1.0718	CAS(5,7)	−92.2844	1.715		1.968	3.664
	CAS(9,9)	−92.3471	2.275	3.452	1.598	3.510
1.1718 equilibrium	HF	−92.2174			2.261	2.645
	CAS(5,7)	−92.3070	0.955		1.890	3.826
	CAS(9,9)	−92.3772	1.613	3.575	1.433	3.583
	R-matrix [9]	−92.3810	1.515	3.491	1.612	3.407
	Expt.		1.151 [31]	3.197 [31]	1.45 [32]	3.862 ± 0.004 [33]
1.2718	CAS(5,7)	−92.2887	0.318		1.715	3.953
	CAS(9,9)	−92.3662	1.082	3.628	1.279	3.617
1.3718	CAS(5,7)	0.519	−92.2636		0.093	3.823
1.4718	CAS(5,7)	1.540	−92.2443		0.058	3.290
1.5718	CAS(5,7)	1.597	−92.2145		0.213	3.038
1.6718	CAS(5,7)	1.548	−92.1849		0.350	2.779

used to obtain the scattering observables and the various scattering cross sections. Eigenphases are obtained by diagonalizing the K-matrix, which are used to determine resonance parameters.

3. Calculation details

3.1. Target models

CN radical has 13 electrons; it is a linear open-shell molecule belonging to the $C_{\infty v}$ point group. Here molecule is treated in the lower symmetry C_{2v}, as QEC [27] in common with nearly all other electronic structure codes, only provides Abelian point group symmetries. The main configuration of the initial $X\,^2\Sigma^+$ electronic ground state is $1\sigma^2 2\sigma^2 3\sigma^2 4\sigma^2 1\pi^4 5\sigma^1$, and the $A\,^2\Pi$ electronic excited states are described as $1\sigma^2 2\sigma^2 3\sigma^2 4\sigma^2 1\pi^3 5\sigma^2$. We perform state-averaged complete active space self-consistent field (SA-CASSCF) calculations with a cc-pVTZ basis set to generate molecular target orbitals for the following close-coupling (CC) scattering calculations. Several complete active space configuration-interaction (CAS-CI) calculations were tested to ensure we have a robust representation of low-energy electron scattering from CN. As the target model is improved the corresponding scattering model becomes computationally more expensive and ultimately unmanageable. Considering the target description accuracy and computational resources, finally we present results of calculations generated using two CAS-CI models for comparison. In first, CAS(5, 7) model, eight core electrons were frozen in doubly occupied 1σ, 2σ, 3σ and 4σ molecular orbitals and five valence electrons are distributed in the 5σ, 6σ, 7σ, 1π and 2π valence molecular orbitals, and this model can represent a wide range of internuclear separations. Alternatively, four core electrons were put into in doubly occupied 1σ and 2σ molecular orbitals, and remaining nine valence electrons move freely in a complete active space which also includes the 6σ, 7σ and 2π virtual orbitals, described as the CAS(9, 9) model. A total of 71 CN geometries with $0.9718 \leqslant R \leqslant 1.6718$ Å on a grid of 0.01 Å were considered in the CAS(5, 7) calculations, while four structures with $0.9718 \leqslant R \leqslant 1.2718$ Å and a grid of 0.1 Å were computed at the computationally-expensive CAS (9, 9) level. In the CC scattering model, between 20 and 66 target electronic states are considered in the CAS(5,7) model, and 29 to 39 for the CAS(9,9) model, depending on internuclear separation (R). For the equilibrium structure, $R_e = 1.1718$ Å, we also provide a calculation using Hartree–Fock (HF) target orbitals computed with a cc-pVTZ basis set, and a static exchange (SE) level scattering calculation.

Table 1 gives the ground target energies, excitation energies, ground dipole moments and electron affinities at a range of R. At R_e, it can be shown that our results in the target CAS (9, 9) calculation compare very well with the results of Harrison and Tennyson [9] which were obtained using natural orbitals with an aug-cc-pVTZ basis set. It is necessary to consider the CN target properties, particularly its permanent dipole moment, as dipole interactions dominate the low-energy electron scattering process. The deviation of the ground dipole moment between the CAS(9,9) calculation and the experimental value [32] is only 0.017 D, indicating that all the scattering results based on this model are theoretically more accurate than those of CAS (5, 7) orbitals. The adiabatic electron affinity of 3.826 eV at the CAS(5,7) level is closer to the adiabatic experimental data of 3.862 ± 0.004 eV [33] than that of CAS(9,9) result. The first vertical excitation energy of 0.955 eV at the CAS(5,7) level agrees well with the adiabatic experimental value of 1.151 eV [31]. The adiabatic electron affinities are in the

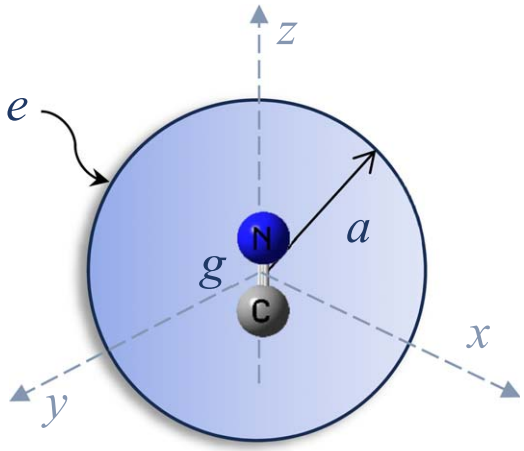

Figure 1. The space of electron scattering on CN radical is divided into an inner region and an outer region by R-matrix method, and the boundary is given by a sphere of radius $a = 10\,a_0$ centered on the target center-of-mass of g.

range of 2–4 eV for all the geometries considered. Our calculations also find that the $A\,^2\Pi$ state becomes the electronic state with the lowest target energy for $R > 1.2718$ Å.

3.2. Scattering models

Having constructed a reliable target model, several scattering models can be tested by use of appropriate choices in equation (1). The simplest model, static exchange (SE) approximation, uses only the Hartree–Fock ground state target wave function, thus the SE model is only capable of describing elastic scatterings and shape resonances. More sophisticated models, the CC approximation, includes a number of ground and excited electronic states, which are represented by a configuration interaction (CI) expansion. This approximation level can give accurate description of excitation cross sections especially in the low energy ranges, and therefore are very suitable for studying different types of resonances. The CC scattering model was used to study resonances and cross sections as a function of R for this work. The calculations are performed by invoking the fixed nuclei approximation. This corresponds to the neglect of nuclear motion and therefore all the calculated quantities depend parametrically on R. For different R, the molecular CN axis is fixed in the z direction but the partial wave expansion used to represent the scattering wavefunction ensures that collisions electrons in all orientations are considered; this allows differential and momentum transfer cross sections to be computed. Hartree–Fock and SA-CASSCF orbitals obtained from the above target models were used in SE and CC scattering calculations, respectively. Specifically, the electron-CN scattering channels investigated in the present work are listed below:

$$\begin{aligned}
&e^- + \mathrm{CN}\,(\text{target state}) \rightarrow \mathrm{CN}^-\,(\text{resonant state}) \rightarrow e^- + \mathrm{CN}\,(\text{scattering state})\\
&\text{elastic } e^- + \mathrm{CN}\,(X\,^2\Sigma^+) \rightarrow e^- + \mathrm{CN}\,(X\,^2\Sigma^+)\\
&\text{electronic excitation } e^- + \mathrm{CN}\,(X\,^2\Sigma^+) \rightarrow e^- + \mathrm{CN}^*\,(A\,^2\Pi \text{ and } B\,^2\Sigma^+)
\end{aligned}$$

We choose an R-matrix radius of $a = 10\,a_0$ for the scattering calculations, see figure 1, and use a compact cc-pVTZ GTO basis set to represent the target. Use of a larger radius, $a = 14\,a_0$, made little difference to the scattering results in test calculations with a cc-pVDZ basis set. In order to represent the scattering electron, we included continuum orbitals as bond-centred GTOs fitted to Bessel functions with $l \leqslant 4$ [34]. The higher partial waves are included in the scattering T-matrices via analytic Born T-matrices to ensure the effect of rotation involved; a similar approach [35] was used to Born-corrected the electronic excitation cross sections considered here which are both dipole-allowed. Program RESON [36] was used to automatically detect and fit resonances using a Breit−Wigner profile. A resonance appears in the eigenphase sum as a jump of approximately π radians, that reflects the resonance position. Differential and momentum transfer cross sections were generated using program POLYDCS [37]; this code allows for the explicit inclusion of rotational motion which is particularly important for a dipolar system such as CN [38].

4. Results and discussion

4.1. Resonances

Resonances form an important feature of low-energy scattering as their presence leads to greatly enhanced vibrational excitation cross sections and the possibility of dissociative electron attach leading to a neutral and an

Table 2. Resonance positions and widths (in eV) for CN radical in the CC calculations with CAS(5,7) and CAS(9,9) target molecular orbitals. *a* indicates a manual fit from [9].

R (Å)	Method	$^3\Sigma^+$	$1\,^3\Pi$	$2\,^3\Pi$	$^3\Sigma^-$	$^1\Sigma^-$
0.9718	CAS(5,7)	6.338 (1.754)			7.270 (2.248)	7.989 (2.656)
	CAS(9,9)	6.826 (1.561)		8.001 (2.309)	7.723 (1.957)	8.646 (2.560)
	R-matrix [9]	7.55 (2.01)		9.72	9.04 (2.89)	
1.0718	CAS(5,7)	4.282 (1.054)			5.300 (1.488)	6.054 (1.688)
	CAS(9,9)	4.685 (0.873)		6.943 (1.486)	5.779 (1.257)	6.648 (1.558)
	R-matrix [9]	5.71 (1.35)		7.76 (3.14)	6.64 (1.73)	
1.1718 equilibrium	CAS(5,7)	2.542 (0.521)	3.087 (1.173)		3.569 (0.942)	4.416 (1.093)
	CAS(9,9)	2.974 (0.357)	2.943 (0.978)	6.256 (0.841)	4.155 (0.821)	4.918 (0.915)
	R-matrix [9]	4.526 (1.186)	3.208 (1.084)		4.881 (1.084)	
	CCSD [12]	2.35 (0.20)	2.63 (0.61)		4.19 (0.64)	4.3 (0.65)
1.2718	CAS(5,7)	1.134 (0.209)	2.261 (0.648)		2.059 (0.476)	3.047 (0.749)
	CAS(9,9)	1.692 (0.116)	2.175 (0.589)	5.714 (0.496)	2.778 (0.425)	
	R-matrix [9]	2.08 (0.25)	2.64 (0.84)		4.1*a*	
1.3718	CAS(5,7)	0.176 (0.021)	2.226 (0.331)		1.085 (0.208)	2.127 (0.483)
	R-matrix [9]	1.03 (0.08)	2.08 (0.52)		2.40 (0.43)	
1.4718	CAS(5,7)		2.457 (0.116)			
1.5718	CAS(5,7)		2.023 (0.035)			
1.6718	CAS(5,7)		1.587 (0.009)			

anionic fragment. Table 2 gives the CN^- resonance positions and widths at a range R calculated using the CC model with target molecular orbitals of CAS(5,7) and CAS(9,9). It is notable that there are no resonances present in our SE calculations. We find five resonances at R_e, namely $1\,^3\Pi$, $^3\Sigma^+$, $^3\Sigma^-$, $^1\Sigma^-$ and $2\,^3\Pi$ in energy order., We distinguish two $1\,^3\Pi$ and $2\,^3\Pi$ resonant states at the CAS(9,9) level, compared to the single $^3\Pi$ symmetry resonance given by Harrison and Tennyson [9]. As the second $2\,^3\Pi$ resonance is located at high energy, it is difficult to detect this new resonant state using the CAS(5,7) target model. The present results for CN^- can be related to the electronic structure of isoelectronic diatomic molecule, N_2. All predicted CN^- resonance symmetries follow closely the corresponding energy order of N_2 low-lying excited electronic states [24] with same symmetries. At R_e, the $1\,^3\Pi$ resonance energy in the CAS(9,9) calculation is 0.265 eV lower than the value given by Harrision and Tennyson [9]. Indeed, once we adjust for the fact that Skomorowski *et al* [12] use the CN^- bound state as their zero of energy (a shift of 3.99 eV at R_e), there is a reasonable correspondence between the position and width of the $^3\Sigma^+$, $1\,^3\Pi$, $^3\Sigma^-$ and $^1\Sigma^-$ resonances, between our calculations at R_e and the result of Skomorowski *et al* [12]. In particular, our $^3\Sigma^-$ with position of 4.155 eV for the CAS(9,9) level matches the resonance energy of 4.19 eV calculated by Skomorowski *et al* [12] very well.

In order to explore the CN^- resonant and bound properties, we extend our analysis on the behavior of the $^3\Sigma^+$, $^3\Sigma^-$, $^1\Sigma^-$ and $1\,^3\Pi$ resonance symmetries with geometry grid of 0.01 Å from the R-matrix with CAS(5,7) described above in figures 2 and 3. The complete resonance and potential energy curves are given in the supplementary material. On the whole, the resonance energies obtained from CAS(5,7) level lies at lower energy than the CAS(9,9) calculation results for different target structures, except for $1\,^3\Pi$ resonant state at 1.1718 and 1.2718 Å. The resonance widths in the CAS(5,7) calculations are broader than the results of the CAS(9,9) model. Combining table 2 and figure 2, these resonance widths appear to be strongly dependent on R. The four resonant widths increase with the decreasing R; that such broad resonances eventually become undetectable at short bond lengths. Conversely at large R, electron collisions with the stretched CN molecule leads to the formation of long-lived CN^- anions which turn into stable valence bound states (i.e. states of zero width) upon crossing the target curve. It would appear that 3 of the 4 resonances depicted in figure 2 do indeed become bound. These four resonance position curves show a small jump at around 1.2818 Å which corresponds to the crossing point between the ground $X\,^2\Sigma^+$ and $A\,^2\Pi$ electronic states; and there is one additional jump at 1.4318 Å for $^3\Pi$ symmetry. The discontinuities in the resonance position are associated with the underlying target electronic structure at these geometries. The potential energy curves of CN target electronic states, computed point by point at the CAS(5,7) level, are not continuous at 1.2818 Å and 1.4318 Å using the underlying Molpro program run from the QEC code. Failure to detect the $^3\Sigma^-$ and $^1\Sigma^-$ resonances beyond 1.4 Å internuclear distances is also probably due to the limitations of our resonance fitting procedure.

The CN molecular potential energies of the lowest two $X\,^2\Sigma^+$ and $A\,^2\Pi$ electronic states are calculated using multi-reference configuration interaction (MRCI) approach with aug-cc-pVTZ basis set in figure 3. The four CN^- potential energy curves are obtained by adding the ground target state energy to the resonance position at each R. In addition, the bound $^3\Sigma^+$ potential curve at large R comes from an MRCI calculation performed with Molpro which extends the curve to its asymptotic limit. This curve matches the resonance curve well at the

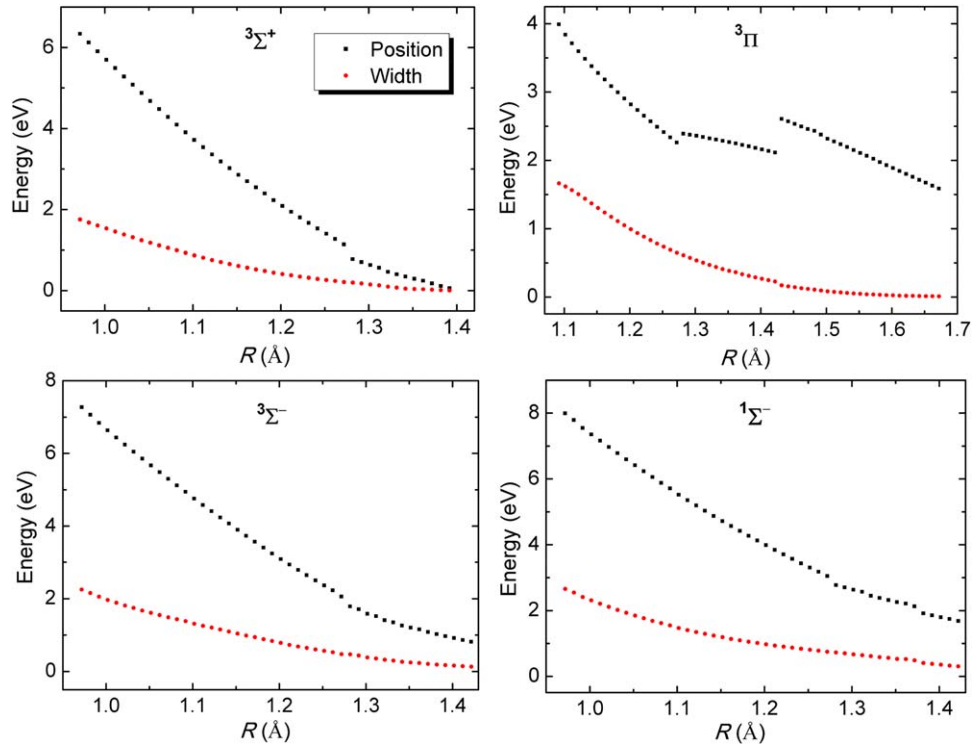

Figure 2. Electron-impact CN^- resonance positions (black dots) and widths (red dots) with Σ and Π symmetries as a function of changing internuclear distances (*R*).

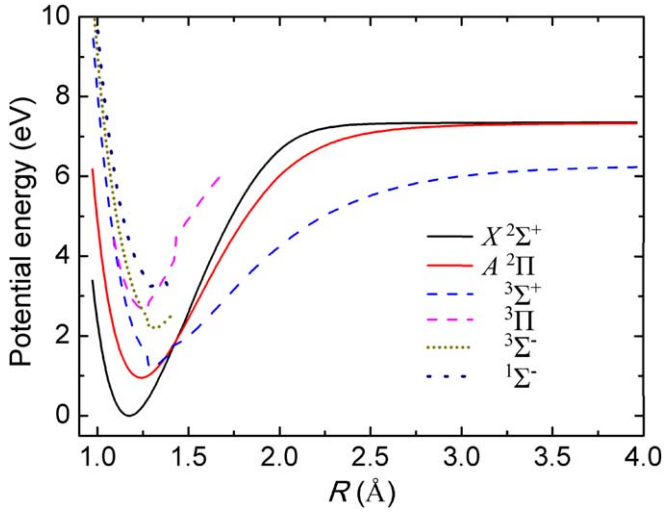

Figure 3. Comparison of potential energy curves for the CN ground $X\,^2\Sigma^+$ and $A\,^2\Pi$ electronic states (solid lines) along with the CN^- resonance energy curves with Σ and Π symmetries (dashed lines). Resonance energies below the corresponding ground state energies represent the formation of CN^- bound state.

crossing point. As N does not have a bound anionic state, one can assume that the asymptote is $C^- + N$; our curve give an asymptotic electron affinity of 1.09 eV, in reasonable agreement with the experimental value of 1.26 eV for carbon atom [39]. It can be seen that we successfully performed $^3\Pi$, $^3\Sigma^-$ and $^1\Sigma^-$ resonant states calculations up $R = 1.6718$, 1.4218 and 1.4218 Å, respectively. For the $^3\Sigma^+$ resonance in figure 2, it disappears at *R* beyond 1.3918 Å, which is exactly the crossing point between the curves of $^3\Sigma^+$ resonance state and lowest ground $A\,^2\Pi$ target state, then becomes a stable bound at large *R* as shown in figure 3. Although the trend of the other three resonance curves is not clear at large *R*, the $^3\Sigma^-$ and $^1\Sigma^-$ appear to going to cross the target state and become bound states.

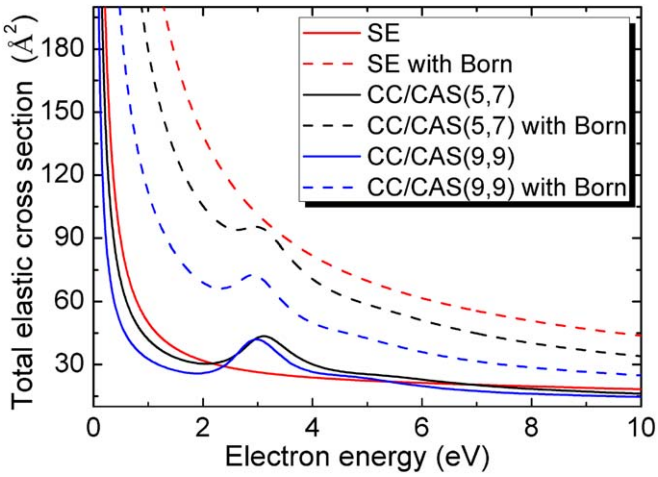

Figure 4. Total elastic cross sections of $X\,^2\Sigma^+ \rightarrow X\,^2\Sigma^+$ for CN radical with and without Born corrections at R_e using different scattering models.

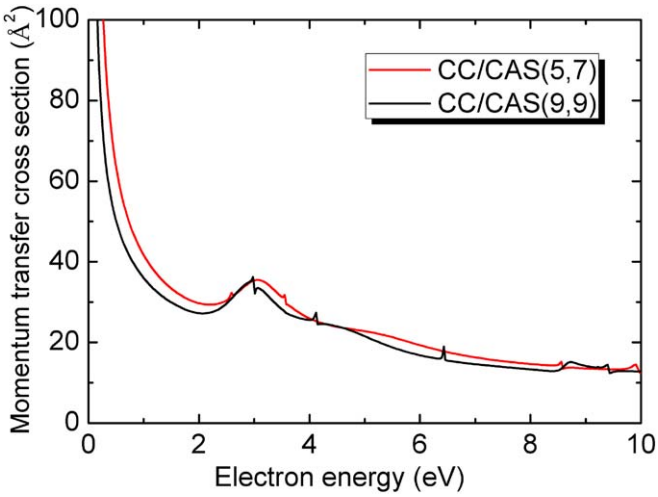

Figure 5. Momentum transfer cross sections for elastic scattering of electrons by CN radical at R_e computed using the CC model.

Comparison of our resonances with those given by Skomorowski *et al* [12] shows the quantitative consistency between our R-matrix and their CCSD calculations. Skomorowski *et al* [12] analyzed these resonances and categorized them all as typical shape resonances, as they claimed all resonant states can decay to the $^2\Sigma^+$ or $^2\Pi$ parent radicals in a one electron process. A shape resonance is formed by an electron attaching to a molecule in its ground electronic state, usually at incident electron energies below the first target excited threshold energy. However, all our resonances lie above the first $A\,^2\Pi$ or $X\,^2\Sigma^+$ excited state for each geometry as shown in tables 1 and 2. Moreover, we did not detect any resonances using the SE model which should capture shape resonances. Feshbach resonance can the thought of as core-excited resonance which lie below their parent target state; they generally lifetimes than core-excited shape resonance as they cannot auto-ionize to give heir parent target state. At R_e in table 2, nearly all the R-matrix calculated resonances present very broad widths with around 1 eV. Thus the five resonances can be reasonably classified as core-excited shape resonance.

4.2. Elastic and inelastic cross sections

The elastic and electronic excitation cross section results are discussed in this section. Various calculated levels are compared to get the reliable values as there are no experimental results available in the literature. We first discuss total elastic cross sections (TECS), momentum transfer cross sections (MTCS) and differential cross sections (DCS) for CN radical in the R_e, and we also compare cross section curves at several internuclear separations based on CC with CAS(9,9) orbital calculations. At R_e, the TECS in figure 4 and MTCS in figure 5 overall decrease as incident electron energy increases. Especially our cross section curves become flat beyond 4

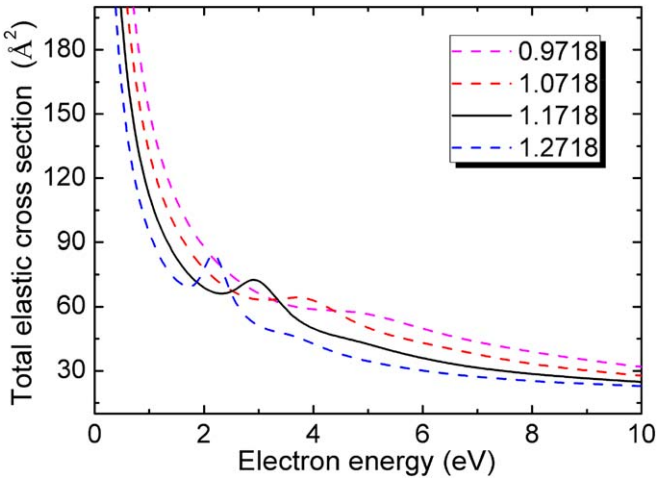

Figure 6. Comparison of total elastic cross sections with different R (in Å) obtained using the CC model at the CAS(9,9) level.

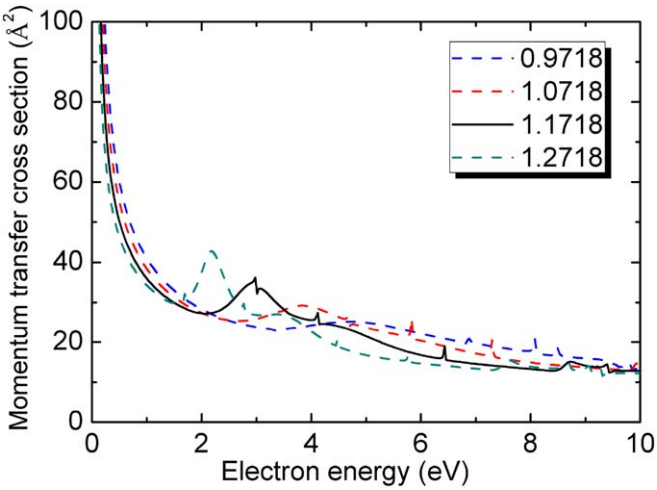

Figure 7. Comparison of momentum transfer cross sections for different R (in Å) obtained using the CC model at the CAS(9,9) level.

eV which is in good agreement with the elastic cross section of Harrison and Tennyson [9], presumably due to the formation of stable bound state with electron affinity of around 3.8 eV as shown in table 1. There is a prominent peak at 3 eV from TECS and MTCS in the CC calculations, which is a reflection of the $^3\Sigma^+$ and 1 $^3\Pi$ resonance states. Figure 5 shows there are also two weak humps for MTCS located at 4.1 eV and 6.5 eV which can be respectively associated with the $^3\Sigma^-$ of 4.155 eV and 2 $^3\Pi$ of 6.256 eV at CC/CAS(9,9) level. The TECS obtained from SE model are very smooth which means there are no indications of a resonance over the whole range. Moreover, it is found that inclusion of the effect of higher partial waves using the Born correction leads to significant increases in the TECS. Particularly the magnitude of Born-corrected TECS at all energies is about three times larger than the corresponding TECS without correction for the SE level calculation. In general, the CC/CAS (5,7) calculations possibly overestimate the elastic cross section in the low energy region, as this model yields larger ground state dipole than those of CC/CAS (9,9) calculations as shown in table 1.

As the R increases, the peaks in the TECS shown in figure 6 and MTCS in figure 7 get higher and the corresponding electron energies become lower, which is consistent with the trend in the resonance energies. Moreover, the weak humps between 2 eV and 8 eV for MTCS in figure 5 are closely related to the resonances obtained in table 2. Above 8 eV, our CC calculations may be suffer from the presence of pseudo resonances which appear as very narrow spikes in the MTCS.

The DCS at R_e shown in figure 8 generally decrease with increasing incident energy or scattering angle. At 1 eV, the calculated DCS from the CC/CAS(5,7) level are slightly higher than that of the CC/CAS(9,9) model for

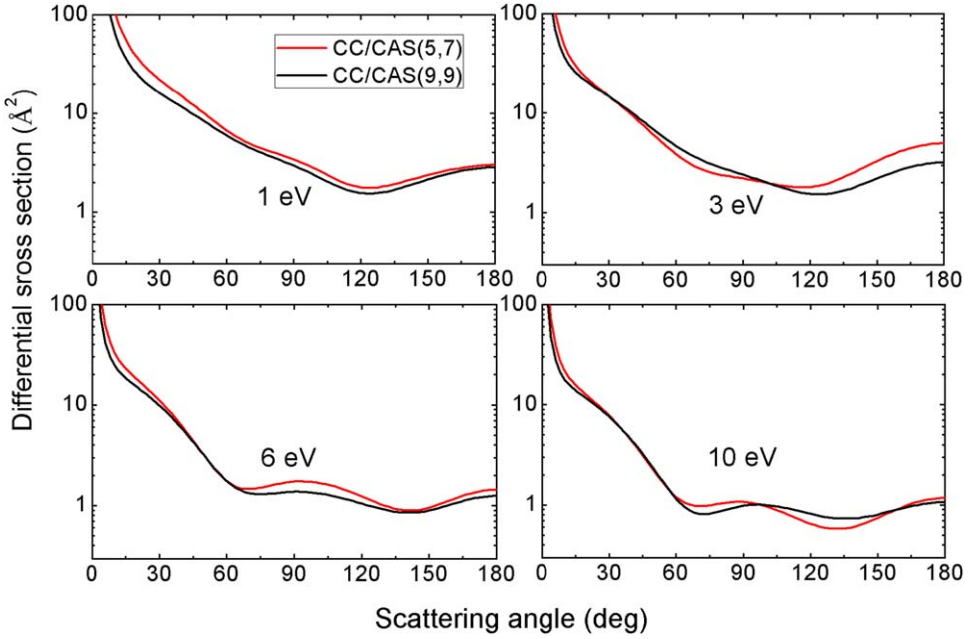

Figure 8. Elastic differential cross sections for incident energies of 1, 3, 6 and 10 eV at R_e obtained from the CC model.

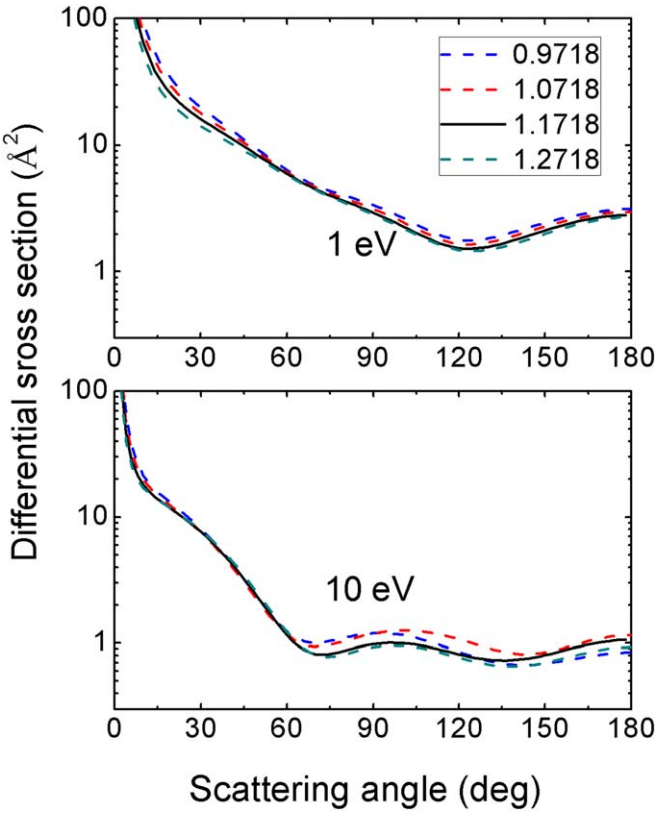

Figure 9. Comparison of differential cross sections at the incident energies of 1 and 10 eV with different R (in Å) obtained using the CC model at the CAS(9, 9) level.

all scattering angles. We note that the DCS curves tend to be flat for scattering angles above 60° with increasing incident energy. Conversely, below 60°, the DCS rapidly increase as the scattering angle tends to zero, and the distribution characteristics is consistent with scattering from a dipolar molecule. Our DCS calculated results with different R nearly overlap each other in figure 9, especially at the low incident energy of 1 eV.

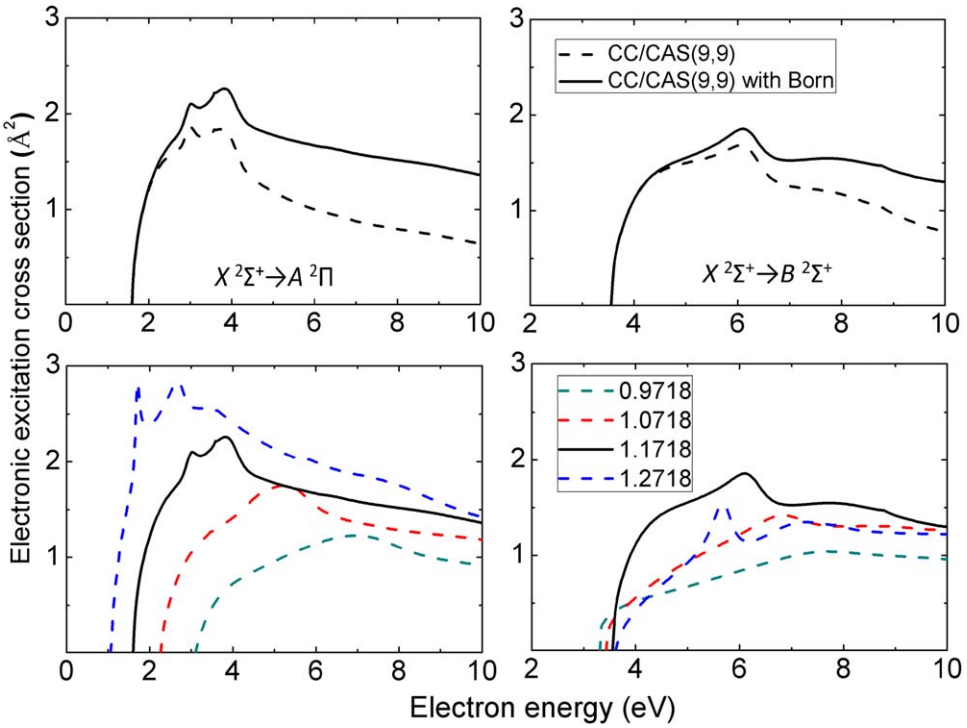

Figure 10. Electron impact electronic excitation cross sections of $A\,^2\Pi$ and $B\,^2\Sigma^+$ states at R_e (upper panels) and with different R (in Å) (lower panels) obtained using the Born-corrected CC model at the CAS(9,9) level.

Analysis of the inelastic electronic transition can provide additional information about resonances lying at energies beyond the first vertical excitation energy. Moreover, modelling electronic emission spectra following electron impact excitation requires knowledge of appropriate electronic excitation mechanisms. Here we discuss electronic excitation cross sections on both $A\,^2\Pi$ and $B\,^2\Sigma^+$ excited states from the ground $X\,^2\Sigma^+$ state using CC model with CAS(9,9) level. The excitation thresholds shown in figure 10 correspond to the vertical excitation energies given in table 1.

Considering the $X\,^2\Sigma^+ \rightarrow A\,^2\Pi$ and $B\,^2\Sigma^+$ electronic excitation cross sections at R_e shown in the upper panels of figure 10, the Born correction contributes significant especially at energies above the first peak, presumably as high partial waves become increasingly important. Compared to the results from Harrison and Tennyson [9] based on their natural orbital calculations, the magnitude of our cross sections with and without Born corrections are slightly lower, while there are similarities in the shape. For the $A\,^2\Pi$ state, the peak structures of electronic excitation cross section between 2 eV and 4 eV are mainly attributed to the formation of three $^3\Sigma^+$, 1 $^3\Pi$ and $^3\Sigma^-$ symmetry resonances in table 2. We have noticed that the $A\,^2\Pi$ excitation state contributes more than the $B\,^2\Sigma^+$ excitation state especially at the separate peak positions. In addition, the 2 $^3\Pi$ resonance symmetry make largely domination to the $X\,^2\Sigma^+ \rightarrow B\,^2\Sigma^+$ excitation cross section at around 6 eV.

The lower panel of figure 10 shows the differences in electronic transition cross sections as a function of R. The changes are significant for near threshold for excitation to $A\,^2\Pi$ state, and but show less variation for $B\,^2\Sigma^+$ state except for region of the peak positions. Combining with above elastic scattering analysis, we conclude that the R plays an important role in the magnitude of scattering cross sections particularly at the resonance peak positions. For the $X\,^2\Sigma^+ \rightarrow A\,^2\Pi$ excitation process, the cross section generally becomes higher as R increasing, whereas the corresponding peak position decreasing which is in good agreement with the trend of above resonances. There is a very pronounced resonance peak below 1 eV at the bond length of 1.2718 Å for $A\,^2\Pi$ state, which is a reflection of the detected $^3\Sigma^+$ resonance located at 1.692 eV.

5. Conclusions

We investigate in detail a set of resonances along with scattering cross sections for the low-energy electron scattering on open-shell CN radical at the equilibrium and extended target structures. To the best of our knowledge, the momentum transfer and differential cross sections for CN are investigated for the first time. Our previous study [24, 26] on N-containing molecules using the R-matrix approach have shown good agreement of

the cross section with the experimental and theoretical results. In absence of any experiments on electron-CN collisions, this gives us the confidence that the results presented here for CN using a similar methodology are reliable, especially at the high-level CC/CAS(9,9) calculations.

We found five low-lying CN^- resonance states, in energy order $1\,^3\Pi$, $^3\Sigma^+$, $2\,^3\Pi$, $^3\Sigma^-$ and $^1\Sigma^-$ at the equilibrium structure. These metastable states should be classified as core-excited shape resonances rather than shape resonances as suggested before [12]. The $^3\Sigma^+$, $1\,^3\Pi$ and $^3\Sigma^-$ resonances make contributions to the peak structures in the elastic and inelastic scattering processes for the incident energy from 2 to 4 eV. In addition, the $2\,^3\Pi$ resonant state with effect on the inelastic electronic excitation of $X\,^2\Sigma^+ \rightarrow B\,^2\Sigma^+$ are also found, confirming the success of estimating the resonances. Our $A\,^2\Pi$ and $B\,^2\Sigma^+$ excitation cross sections from its ground state using the CC model compares well with those results of Harrison and Tennyson [9] in their high level calculations. Moreover, the magnitude of the elastic cross section is more than ten times larger than the $A\,^2\Pi$ and $B\,^2\Sigma^+$ electronic excitation cross sections, indicating the elastic collisions significantly contribute to the total cross sections in the low energy regions.

All resonances become lower in energy and narrower as the target internuclear separation increases, which is consistent with the trend of changing peak positions in the elastic and electronic excitation cross sections. The $^3\Sigma^+$ symmetry resonance becomes a stable bound state beyond 1.3918 Å. In terms of changing target geometry structures, the difference on cross sections is prominent at the resonance peak positions. In general the effect of including vibrational motion in the treatment of resonances has the effect of spreading out the resonance over a wider range of energies. The resonance is narrow this usually manifests itself as a series of sharp, vibrationally-resolved resonance feature [40]. For broad resonances, the structure is usually partially or mostly washed out [41]. Conversely rotational effects are usually too small to be resolved and are generally assumed to be less important. For further improvements, future work will focus on the electron collision with CN radical involving rotational and vibrational motion, and our resonance curves and widths will be used to investigate electron-impact resonant vibration excitation and dissociative electron attachment.

Acknowledgments

We acknowledge the support from the Chinese Scholarship Council (Grant 202006240163), the support from National Key R&D Program of China (Grant 2017YFA0303600); NSFC (Grant 11974253).

Conflict of interests

The authors declare that there are no conflicts of interests.

Data availability statement

All data that support the findings of this study are included within the article (and any supplementary files).

ORCID iDs

He Su https://orcid.org/0009-0009-6381-2245
Jonathan Tennyson https://orcid.org/0000-0002-4994-5238
Hong Zhang https://orcid.org/0000-0003-3098-7988

References

[1] Leach S 2012 Why COBE and CN spectroscopy cosmic background radiation temperature measurements differ, and a remedy *Mon. Not. R. Astron. Soc.* **421** 1325
[2] Harrison S, Tennyson J and Faure A 2012 *Calculated electron impact spin-coupled rotational cross-sections for 2S+1Σ+ linear molecules: CN as an example J. Phys. B: At. Mol. Opt. Phys.* **45** 175202
[3] Prasad C V V and Bernath P F 1992 *Fourier transform jet-emission spectroscopy of the A2Πi-X2Σ+ transition of CN J. Mol. Spectrosc.* **156** 327
[4] Tokue I and Kuchitsu K 1975 Formation of CN(B2Σ) by the electron impact dissociation of cyanides. rotational energy distribution of CN(B2Σ) from HCN *Chem. Phys. Lett.* **34** 369
[5] Kozlov S V, Terashkevich V A, Pazyuk E A, Stolyarov A V, Yurchenko S N and Tennyson J 2024 An upgraded line list for radiative transitions between the B 2Σ+, A 2Π, and X 2Σ+ states of the CN radical *Astrophys. J. Suppl. Ser.* **275** 29
[6] Agúndez M *et al* 2010 Astronomical identification of CN-, the smallest observed molecular anion *Astron. Astrophys.* **517** 1
[7] Douguet N, Fonseca Dos Santos S, Raoult M, Dulieu O, Orel A E and Kokoouline V 2013 Theory of radiative electron attachment to molecules: benchmark study of CN *Phys. Rev. A* **88** 11

[8] Khamesian M, Douguet N, Fonseca dos Santos S, Dulieu O, Raoult M, Brigg W J and Kokoouline V 2016 Formation of CN-, C3N-, and C5N- molecules by radiative electron attachment and their destruction by photodetachment *Phys. Rev. Lett.* **117** 123001
[9] Harrison S and Tennyson J 2012 Electron collisions with the CN radical: bound states and resonances *J. Phys. B: At. Mol. Opt. Phys.* **45** 035204
[10] Carelli F, Gianturco F A, Wester R and Satta M 2014 Formation of cyanopolyyne anions in the interstellar medium: the possible role of permanent dipoles *J. Chem. Phys.* **141** 054302
[11] Gao X, Xie J, Li H, Meng X, Wu Y and Tian S X 2021 Direct observation of long-lived cyanide anions in superexcited states *Commun. Chem.* **4** 13
[12] Skomorowski W, Gulania S and Krylov A I 2018 Bound and continuum-embedded states of cyanopolyyne anions *Phys. Chem. Chem. Phys.* **20** 4805
[13] Crawford O H, Allison A C and Dalgarno A 1969 Electron impact excitation of CN *Astron. Astrophys.* **2** 451
[14] Allison A C and Dalgarno A 1971 Rotational excitation of CN by electron impact *Astron. Astrophys.* **13** 331
[15] Pandya S H, Shelat F A, Joshipura K N and Vaishnav B G 2012 Electron ionization of exotic molecular targets CN, C2N2, HCN, HNC and BF- Theoretical cross sections *Int. J. Mass spectrom.* **323–324** 28
[16] Tennyson J 2010 Electron-molecule collision calculations using the R-matrix method *Phys. Rep.* **491** 29
[17] Burke P G 2011 *R-Matrix Theory of Atomic Collisions* (Springer) (https://doi.org/10.1007/978-3-642-15931-2)
[18] Harrison S, Faure A and Tennyson J 2013 CN excitation and electron densities in diffuse molecular clouds *Mon. Not. R. Astron. Soc.* **435** 3541
[19] Derouich M, Mustajab F, Qutub S and Ahmad B Z 2020 Depolarizing isotropic collisions of the CN solar molecule with electrons *Res. Astron. Astrophys.* **20** 210
[20] Padellec A L *et al* 2001 Electron scattering on CN *Phys. Scr.* **64** 467
[21] Andersen L H, Bak J, Boyé S, Clausen M, Hovgaard M, Jensen M J, Lapierre A and Seiersen K 2001 Resonant and nonresonant electron impact detachment of CN- and BO *J. Chem. Phys.* **115** 3566
[22] Belic D S, Urbain X, Cherkani-Hassani H and Defrance P 2017 Electron-impact dissociation and ionization of CN+ Ions *Phys. Rev. A* **95** 1
[23] Kumar S S, Hauser D, Jindra R, Best T, Roučka Š, Geppert W D, Millar T J and Wester R 2013 Photodetachment as a destruction mechanism for CN- and C3N- anions in circumstellar envelopes *Astrophys. J.* **776** 25
[24] Su H, Cheng X, Zhang H and Tennyson J 2021 Electro collisions with molecular nitrogen in its ground and electronically excited states using the R-matrix method *J. Phys. B: At. Mol. Opt. Phys.* **54** 115203
[25] Su H, Cheng X, Cooper B, Tennyson J and Zhang H 2022 Electron-impact high-lying N2- resonant states *Phys. Rev. A* **105** 062824
[26] Su H, Cheng X, Cooper B, Tennyson J and Zhang H 2023 Elastic and inelastic low-energy electron scattering from pyridine *J. Chem. Phys.* **158** 024301
[27] Cooper B *et al* 2019 Quantemol electron collisions (QEC): an enhanced expert system for performing electron molecule collision calculations using the R-matrix method *Atoms* **7** 97
[28] Werner H-J, Knowles P J, Lindh R, Manby F R, Schütz M *et al* 2020 A package of ab initio programs See (https://molpro.net)
[29] Mašín Z, Benda J, Gorfinkiel J D, Harvey A G and Tennyson J 2020 UKRmol + : a suite for modelling of electronic processes in molecules interacting with electrons , positrons and photons using the R-matrix method *Comput. Phys. Commun.* **249** 107092
[30] Gailitis M 1976 New forms of asymptotic expansions for wavefunctions of charged-particle scattering *J. Phys. B: At. Mol. Phys.* **9** 843
[31] Huber K P and Herzberg G 2025 NIST Standard Reference Database Number 69 *Gaithersburg, MD: National Institute of Standards and Technology* ed P J Linstrom and W G Mallard (NIST Chemistry WebBook) (https://webbook.nist.gov)
[32] Thomson R and Dalby F W 1968 Experimental determination of the dipole moments of the X ($2\Sigma+$) and B ($2\Sigma+$) states of the CN molecule *Can. J. Phys.* **46** 2815
[33] Bradforth S E, Kim E H, Arnold D W and Neumark D M 1993 Photoelectron spectroscopy of CN-, NCO-, and NCS *J. Chem. Phys.* **98** 800
[34] Faure A, Gorfinkiel J D, Morgan L A and Tennyson J 2002 GTOBAS: fitting continuum functions with gaussian-type orbitals *Comput. Phys. Commun.* **144** 224
[35] Kaur S, Baluja K L and Tennyson J 2008 Electron-impact study of NeF using the R -matrix method *Phys. Rev. A* **77** 032718
[36] Tennyson J and Noble C J 1984 RESON-a program for the detection and fitting of breit-wigner resonances *Comput. Phys. Commun.* **33** 421
[37] Sanna N and Gianturco F A 1998 Differential cross sections for electron/positron scattering from polyatomic molecules *Comput. Phys. Commun.* **114** 142
[38] Zhang R, Faure A and Tennyson J 2009 Electron and positron collisions with polar molecules: studies with the benchmark water molecule *Phys. Scr.* **80** 015301
[39] Johnson III R D and NIST Computational Chemistry Comparison and Benchmark Database 2022 NIST Standard Reference Database Number 101, Release 22
[40] Stibbe D T and Tennyson J 1997 Ab initio calculations of vibrationally resolved resonances in electron collisions with H2, HD and D2 *Phys. Rev. Lett.* **79** 4116
[41] Laporta V, Cassidy C M, Tennyson J and Celiberto R 2012 Electron-impact resonant vibration excitation cross sections and rate coefficients for carbon monoxide *Plasma Sources Sci. Technol.* **21** 045005